Version 3 as of July 20, 2008
Primary author: Tim P. Schulze
Submitted to PRE.

Simulation of dendritic growth into an undercooled melt using kinetic Monte Carlo

T.P. Schulze
Mathematics Department 121 Ayres Hall 1403 Circle Drive Knoxville, TN 37996-1300 USA
(Dated: July 20, 2008)

We consider the growth of a single FCC dendrite into an undercooled melt. Unlike most simulations of this well-studied phenomenon, we adopt an atomistic growth model that uses kinetic Monte Carlo to track the free boundary. The model allows for both phase change and exchange between liquid and solid atoms on the surface of the crystal and is coupled to a continuum model for heat transport away from the interface. For small length and time scales, this approach provides simple, effective front tracking with fully resolved atomistic detail. An interesting finding is that the surface exchange mechanism appears to be important for capturing effects due to anisotropy that are needed to produce realistic growth shapes.

PACS numbers: 68.70+w, 68.08-p

The growth of a dendrite into an undercooled melt is a well studied phenomenon, typically modeled from a macroscopic point of view as a Stefan (i.e., free-boundary) problem [1]. For pure materials, morphological instability leading to dendritic growth is the result of interfacial perturbations growing into an environment that is below the material's melting temperature [2]. This enhances the subsequent growth of the perturbations and eventually leads to an intricate, snow-flake like growth pattern. When simulated using continuum models, there are two essential challenges: tracking the free-boundary and resolving the thermal boundary layer ahead of the front. Much effort has gone into each of these issues, with the phase-field [3, 4, 13] and level-set methods [5] featuring prominently in the first, and adaptive mesh techniques [4] and random walks with adaptive step sizes [6] in the second.

In this paper, we focus on the front-tracking problem, adopting a discrete, atomistic model in the spirit of the kinetic Monte-Carlo (KMC) simulations that are popular in the epitaxial growth literature [7]. This approach is closely related to that in [8], where KMC was used to examine the evolution of a Face Centered Cubic (FCC) nano-cluster toward its equilibrium Wulff shape. A number of related studies have examined the growth of simple cubic crystals, starting with work on diffusion limited aggregation [9], continuing with a number of related two-dimensional studies [10], and including at least one study of three-dimensional, simple cubic growth [11]. Here, we consider the combination of growth and surface diffusion for an FCC crystal. For convenience, the interface kinetics are coupled to a continuum model for heat flow, which is then discretized, in both phases, on the same FCC lattice. The aim is to demonstrate that this approach to front-tracking is relatively easy to implement and competitive on scales ranging from nanometers up to several microns while providing a natural way to incorporate both anisotropy and atomistic effects. The model can be extended, as in some of the studies cited above, to consider discrete models for heat flow, allowing for additional effects due to thermal fluctuations.

In the sharp-interface formulation of the continuum model, the computational domain $\Omega \subset \mathbb{R}^3$ is typically decomposed into an inner, solid region Ω_S and an outer, liquid region $\Omega \backslash \Omega_S$, separated by a closed surface $\partial\Omega_S$. The principal governing equation is the heat equation, with the outer boundary $\partial\Omega$ held at a fixed temperature $T_B < T_M$, the temperature of the solid–liquid interface determined by the Gibbs–Thompson equation, and the interface motion determined by a Stefan condition that balances the latent heat release with the heat flux away from the interface:

$$\partial_t T = \kappa \nabla^2 T, \quad \mathbf{x} \in \Omega, \tag{1}$$

$$T = T_B, \qquad \mathbf{x} \in \partial\Omega, \tag{2}$$

$$T = T_M - \frac{\gamma T_M}{\rho L} \nabla \cdot \hat{\mathbf{n}}(\mathbf{x}), \quad \mathbf{x} \in \partial\Omega_S, \tag{3}$$

$$\rho L v_{\hat{\mathbf{n}}} = k \left(\nabla T \cdot \hat{\mathbf{n}}|_S - \nabla T \cdot \hat{\mathbf{n}}|_L \right), \quad \mathbf{x} \in \partial\Omega_S. \tag{4}$$

The thermal diffusivity κ and density ρ have been assumed to be the same in both phases, $\hat{\mathbf{n}}$ is the normal pointing into the liquid, $k = \kappa \rho c_p$ is the thermal conductivity, L the latent heat released per unit mass, and $v_{\hat{\mathbf{n}}}$ is the normal velocity of the interface. The interfacial temperature is given by the equilibrium melting temperature for a flat interface T_M modified by a curvature term accounting for surface energy (the Gibbs-Thompson effect.) With the unit normal pointing into the liquid, a spherical region has positive mean curvature and a lower equilibrium melting temperature. After scaling lengths on the distance between neighboring lattice sites a, time with the thermal diffusion time scale a^2/κ, and temperature with $\Delta T = T_M - T_B$, there are two principal parameters (in the absence of anisotropy)—a surface energy parameter Γ and the Stefan number S:

$$\Gamma = \frac{\gamma T_M}{a \rho L \Delta T}, \quad S = \frac{L}{c_p \Delta T}.$$

In the discrete model, the Stefan number is related to the attachment rate and surface energy can be included by making the melting temperature depend on the number of solid phase nearest neighbors. Other effects, such as kinetic undercooling for a rapidly solidifying interface can also be included. The surface energy γ and diffusivity κ are often modified to model anisotropy by making them a function of orientation. Indeed, this is essential for producing realistic results with the continuum model [13]. In the discrete model, one might have thought that the underlying lattice would play this role, but we find that it is also essential to include a surface exchange process that conserves the number of atoms of each phase while allowing the shape of the interface to change.

The FCC lattice can be defined using integer combinations $\mathbf{x}_{ijk} = i\mathbf{a} + j\mathbf{b} + k\mathbf{c}$ of three basis vectors

$$\mathbf{a} = \frac{\hat{\mathbf{i}} + \hat{\mathbf{j}}}{\sqrt{2}} \times a, \quad \mathbf{b} = \frac{\hat{\mathbf{i}} + \hat{\mathbf{k}}}{\sqrt{2}} \times a, \quad \mathbf{c} = \frac{\hat{\mathbf{k}} + \hat{\mathbf{j}}}{\sqrt{2}} \times a,$$

that are themselves formed by combinations of Cartesian unit vectors $\hat{\mathbf{i}}$, $\hat{\mathbf{j}}$, and $\hat{\mathbf{k}}$ and the equilibrium distance between two atoms a. In practice one need only store and manipulate integer triples (i, j, k), converting to Cartesian coordinates for visualization. Upon scaling, $\{\mathbf{a}, \mathbf{b}, \mathbf{c}\}$ become unit vectors and it is useful to expand this set to the twelve vectors

$$\{\mathbf{e}_i\}_{i=1}^{12} = \{\pm\mathbf{a}, \pm\mathbf{b}, \pm\mathbf{c}, \pm(\mathbf{a}-\mathbf{b}), \pm(\mathbf{b}-\mathbf{c}), \pm(\mathbf{c}-\mathbf{a})\}$$

that point to the nearest neighbors of a given lattice site, storing them in the skewed coordinate system, so that they have integer components.

The solid atoms are constrained to lie on the FCC lattice and the heat equation is solved numerically using a discretization on this same lattice in *both* phases. Like any Ising model, we use an order parameter $\sigma_{ijk} \in \{0, 1\}$, to specify liquid (0) or solid (1) phase. In addition to this phase configuration, we associate a temperature T_{ijk} with each lattice point. Together, σ and $\mathbf{T}$ specify the system state, which will evolve through a combination of thermal diffusion and a stochastic model for surface evolution.

The solidification model is analogous to the combination of the Gibbs-Thompson equation (3) and the Stefan condition (4.) The former suggests associating a melting temperature $T_I(N_{ijk}) = 1 + \tilde{\Gamma}(N_{ijk} - 3)$ with each lattice site, where N_{ijk} is the number of solid nearest neighbors, temperature has been scaled and translated so that $T_M = 1$, and $\tilde{\Gamma}$ is the surface energy parameter identified above times an unspecified geometric factor that translates coordination number into a measure of curvature. Note that T_M is taken to be the melting temperature of the (111)-facet, as most atoms will solidify/melt along such facets when they have three nearest neighbors. We assume that liquid sites below this temperature and solid sites above this temperature are susceptible to phase change, but neglect nucleation (which is equivalent to setting $T_I(0) = -\infty$ and $T_I(12) = \infty$.) For the problem of solidification into an undercooled melt specified above, only freezing will occur.

Liquid sites with temperatures $T_{ijk}^{n+1} < T_I$ have their temperatures pinned at T_I. Thus, these sites serve as sources of latent heat. In the continuum model, the Stefan condition (4) governs the amount of heat needed to convert the phase of such atoms. In the simulations presented below, this condition is enforced in the mean by setting the solidification rate to

$$q_{ijk}^S = \begin{cases} J(\mathbf{x}_{ijk}), & \text{if } \sigma_{ijk} = 0 \ \& \ N_{ijk} > 0 \\ 0, & \text{otherwise} \end{cases},$$

where J (see 6 below) represents the net heat loss at site $\mathbf{x}_{ijk}$ measured in units of latent heat release per atom upon solidification. After an atom has solidified, the constraint on its temperature is released. The model can be modified so that heat is strictly conserved by coupling the growth model to a discrete model for heat transfer.

Anisotropy is included in the model as a surface diffusion process where solid atoms in contact with one or more liquid sites are susceptible to exchange with liquid sites that have at least one additional solid neighbor. This latter rule is similar to what is called the "solid-on-solid" (SOS) assumption in the epitaxy literature and prevents most detachments. Upon exchange, the liquid site retains its (previously constrained) temperature value and the solid site becomes a solidification site with an appropriately constrained melting temperature. Following the standard practice for surface diffusion used in epitaxial growth simulations, we set the hopping rates

$$q_{ijk}^H = \begin{cases} \nu e^{-\Delta E/k_B T}, & \text{if } \sigma_{ijk} = 1 \ \& \ N_{ijk} < 12 \\ 0, & \text{otherwise} \end{cases},$$

where the prefactor $\nu \approx 10^{13}$ hz is an attempt frequency that depends weakly on temperature, but is usually modeled as a constant, k_B is Boltzmann's constant, and ΔE is an energy barrier that must be overcome in moving from a local energy minimum to an adjacent one in the system's configuration space. We adopt the simple model in [8] with $\Delta E = E_N N_{ijk}$ proportional to the coordination number. This is also a common assumption with SOS models for simple cubic growth because it is extremely fast, has a simple heuristic explanation, uses a minimal set of parameters, and is easily reproduced by others.

We assume that all of the random processes occur independent of one another (i.e., they are Poisson processes.) At each KMC timestep δt_n, a hopping (exchange) or solidification (flip) event is selected with probability proportional to their rates and a random waiting time is associated with the event.

When the accumulated micro-timesteps δt_n exceed a macro-timestep Δt the temperature field is updated, subject to the interfacial constraints described above, using an explicit discritization of (1) tailored to the FCC lattice:

$$T_{ijk}^{n+1} = T_{ijk}^n + \frac{\Delta t}{2}\left(\sum_{m=1}^{12} T^n(\mathbf{x}_{ijk} + \mathbf{e}_m) - 12T_{ijk}^n\right). \quad (5)$$

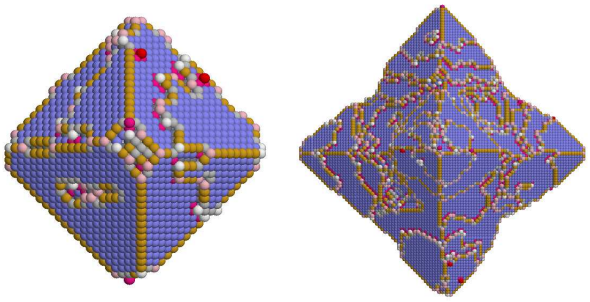

FIG. 1: Two surface images from the early stages of a single simulation, showing about 10^4 (left) and 10^5 (right) atoms colored by coordination number N_{ijk}.

Note that this comes with the severe time-step restriction of $\Delta t \leq 1/6$ for numerical stability. More efficient methods are, however, not so easily adapted to the FCC lattice. For the immediate purpose of studying the merits of KMC as a front-tracking algorithm, we therefore accommodate the time-step restriction by assuming a very small thermal diffusivity and Stefan number. If we take $S^{-1} = 0.9$, for example, we boost the attachment rate of atoms by about three orders of magnitude over more realistic values while staying under the hypercooling threshold $S^{-1} < 1$ [1]. To produce realistic dendrite shapes, we find that we must also boost the hopping rates, controlled by the nondimensional parameter $K = \nu a^2/\kappa$, by a similar order of magnitude.

Note that with the maximum value of the time step $\Delta t = 1/6$, (5) reduces to a simple average over the twelve nearest neighbors and the attachment rate becomes

$$J = S^{-1} \frac{1}{12} \sum_{m=1}^{12} \left[T_I(\mathbf{x}_{ijk}) - T^n(\mathbf{x}_{ijk} + \mathbf{e}_m) \right]. \qquad (6)$$

In practice the time spent tracking the front is small compared to that solving the diffusion equation. Indeed, if, as an experiment, the temperature field is fixed so that it simply decays rapidly with distance from the interface, results qualitatively similar to those shown here can be obtained in minutes rather than hours. In part, this is due to the time step restriction just mentioned, but is also because of an efficiently implemented KMC algorithm described in [12].

For the results presented below, the surface energy parameter is fixed at $\tilde{\Gamma} = 0.01$, the scaled nearest neighbor energy $\tilde{E} = E_N/(k_B T_M) = 0.0034$, and the computational domain is a sphere with a radius 25 times the radius of the initial solid region, a spherical cluster of about 400 atoms. The initial temperature is set to T_M in the solid and T_B in the liquid. We briefly explore the behavior of the growth as the remaining parameter, the surface diffusion prefactor K, is varied. The principal observation is that the strength of this relative to the growth rate controls the extent to which faceting and anisotropy dominate the morphology.

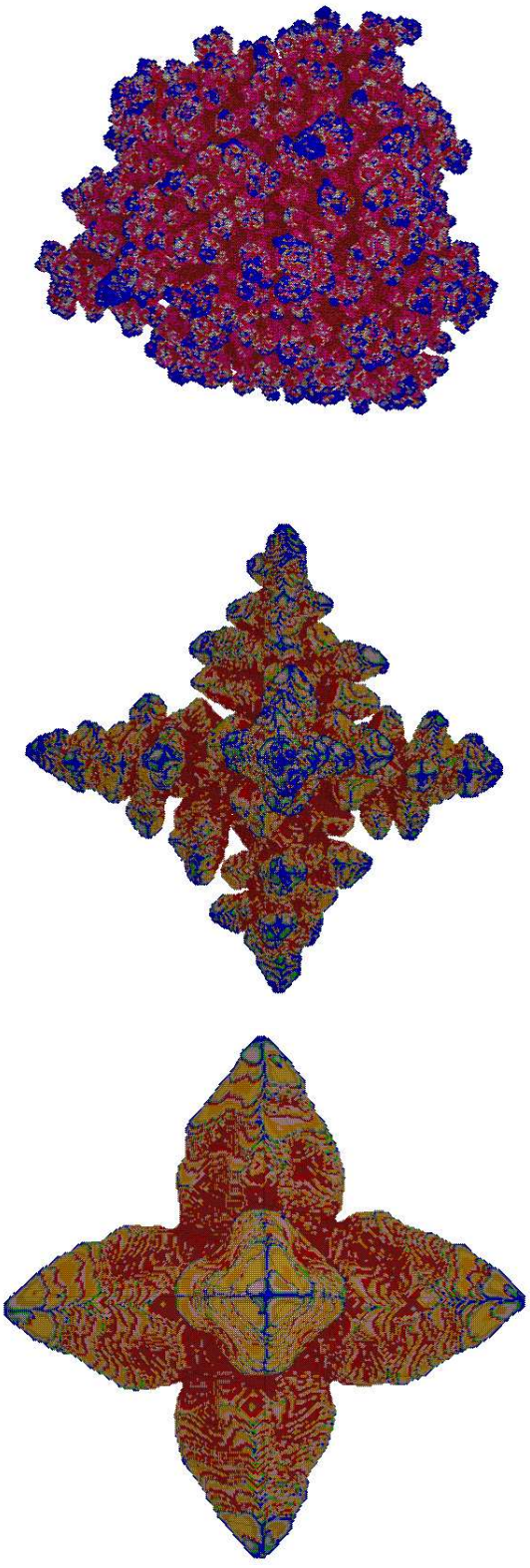

FIG. 2: Three surface images from the late stages of three separate simulations, showing about 10^6 atoms colored by temperature gradient. The rate of surface diffusion is increasing by a factor of ten as you move down the page.

Fig. 1 shows the solid atoms, colored by coordination, that lie on the surface of the crystal. In the first image, the crystal contains about 10^4 atoms and, in the second, there are about 10^5 atoms (the images are not to scale). These images correspond to two times in the same simulation that started from a spherical cluster of about 500 atoms. This simulation had a large value of $K = 10^6$, so that surface diffusion dominates, especially during the early stages of growth, when the surface area is small. In this regime, the crystal grows close to its equilibrium Wulff shape, and the results are similar to that in [8]. The truncated octahedral shape can be understood as a competition between the two slowest growing facets—the (100) and (111) facets, where the diffusing atoms have coordination numbers of four and three, respectively. Note that for an equal number of exposed lattice sites, there would be a net flux of atoms from a (111) facet to a (100) facet, due to the faster hopping rate on the former. Thus, nucleation is favored on the (100) facet. Due to the geometry, each time a layer is completed, a facet shrinks somewhat. The dominance of the (111) facets at early times can therefore be traced back to the slower nucleation rate.

During growth, the surface is nearly isothermal, with $T \approx T_M$. As the crystal becomes larger, the isotherms near protruding regions of the surface become compressed. This effect is most pronounced at the vertices of the octahedral structure. This compression, which implies a steeper temperature gradient, enhances nucleation, and we can see in Fig. 1b that there is a cascade of steps that starts to flow away from the vertices. As the crystal becomes larger, this effect begins to change the morphology of the crystal. In particular, note that the edges are no longer straight in Fig. 1b.

In Fig. 2, the solidifying atoms (i.e., liquid atoms on the surface) are colored using the heat flux J_{ijk}. The images shown are from the late stages of several different simulations where the surface diffusion parameters K has been adjusted to exhibit three characteristic morphologies. The lower image correspond to a much later stage of the simulations exhibited in Fig. 1, with more than 10^6 atoms now represented and the instability having produced the primary branches of a dendrite. The branching process occurs at earlier stages of growth if surface diffusion is less active. In Fig. 2b, secondary and nascent tertiary branches have already formed when the crystal is about the same size as that in Fig. 2a. If the surface diffusion rate is dropped another order of magnitude, the dendrite loses its octahedral symmetry and takes on a cauliflower-like appearance.

In summary, KMC appears to be a promising alternative to modeling and simulation of dendritic growth on atomistic scales. Enlarged versions of the images shown here, available from the author, reveal a spectacular amount detail that offers enhanced insight into the growth process. In future work, there is every reason to expect that the range of parameters addressable by this technique can be greatly increased by coupling it to more efficient methods for solving the heat equation.

This research was supported by NSF-DMS-0707443. The author would like to thank Shaun Hendy for helpful discussions related to this work.

[1] S.H. Davis, *Theory of Solidification,* Cambridge University Press (2001).

[2] W.W. Mullins and R.F. Sekerka, J. App. Phys. **34** (1963) 323–329.

[3] W. J. Boettinger, J. A. Warren, C. Beckermann and A. Karma, *Annual Review of Materials Research* **32** (2002) 163–194.

[4] N. Provatas, M. Greenwood, B. Athreya, N. Goldenfeld and J. Dantzig J, *Int. J. Mod. Phys. B* **19** (2005) 4525-4565.

[5] F. Gibou, R. Fedkiw, R. Caflisch and S. Osher, *J. Sci. Comput.* **19** (2003) 183–199.

[6] M. Plapp and A. Karma, *Phys. Rev. Lett.* **84** (2000) 1740–1743; M. Plapp and A. Karma, *J. Comp. Phys.* **165** (2000) 592-619.

[7] A.B. Bortz, M.H. Kalos and J.L. Lebowitz, J. Comput. Phys. **17** (1975) 10–18; M. Kotrla, *Comp. Phys. Comm.* **97** (1996) 82–100.

[8] N. Combe, P. Jensen and A. Pimpinelli, *Phys. Rev. Lett.* **85** (2000) 110–113.

[9] T.A. Witten and L.M. Sander, *Phys. Rev. Lett.* **47** 1400 (1981).

[10] T. Vicsek, *Phys. Rev. Lett.* **53** 2281 (1984); O. Shochet, K. Kassner, E. Ben-Jacob, S.G. Lipson and H. Muller-Krumbhaar, *Physica A* **181** 136 (1992); O. Shochet, K. Kassner, E. Ben-Jacob, S.G. Lipson and H. Muller-Krumbhaar, *Physica A* **187** 87 (1992); R. Harris and M. Grant, *J. Phys. A: Math. Gen.* **23** (1990) 567–571; Y. Saito and T. Ueta, *Phys. Rev. A* **40** (1989) 3408–3419.

[11] L. Jorgenson, R. Harris, M. Grant and H. Guo, *Phys. Rev. E* **47** (1993) 1235–1242.

[12] T.P. Schulze, *J. Comp. Phys.* **227** (2008) 2455-2462.

[13] J.J. Hoyt, M. Asta and A. Karma, *Mat. Sci. Eng. R* **41** 121 (2003).